ISPRS Journal of Photogrammetry and Remote Sensing 118 (2016) 22–36

Contents lists available at ScienceDirect

ISPRS Journal of Photogrammetry and Remote Sensing

journal homepage: www.elsevier.com/locate/isprsjprs

Road centerline extraction from airborne LiDAR point cloud based on hierarchical fusion and optimization

Zhenyang Hui [a], Youjian Hu [a,*], Shuanggen Jin [b], Yao Ziggah Yevenyo [a]

[a] Faculty of Information Engineering, China University of Geosciences, Wuhan 430074, China
[b] Shanghai Astronomical Observatory, Chinese Academy of Sciences, Shanghai 200030, China

ARTICLE INFO

Article history:
Received 23 November 2015
Received in revised form 28 March 2016
Accepted 5 April 2016

Keywords:
Road centerline extraction
Airborne LiDAR point cloud
Skewness balancing
Rotating neighborhood
Hierarchical fusion and optimization

ABSTRACT

Road information acquisition is an important part of city informatization construction. Airborne LiDAR provides a new means of acquiring road information. However, the existing road extraction methods using LiDAR point clouds always decide the road intensity threshold based on experience, which cannot obtain the optimal threshold to extract a road point cloud. Moreover, these existing methods are deficient in removing the interference of narrow roads and several attached areas (e.g., parking lot and bare ground) to main roads extraction, thereby imparting low completeness and correctness to the city road network extraction result. Aiming at resolving the key technical issues of road extraction from airborne LiDAR point clouds, this paper proposes a novel method to extract road centerlines from airborne LiDAR point clouds. The proposed approach is mainly composed of three key algorithms, namely, Skewness balancing, Rotating neighborhood, and Hierarchical fusion and optimization (SRH). The skewness balancing algorithm used for the filtering was adopted as a new method for obtaining an optimal intensity threshold such that the "pure" road point cloud can be obtained. The rotating neighborhood algorithm on the other hand was developed to remove narrow roads (corridors leading to parking lots or sidewalks), which are not the main roads to be extracted. The proposed hierarchical fusion and optimization algorithm caused the road centerlines to be unaffected by certain attached areas and ensured the road integrity as much as possible. The proposed method was tested using the Vaihingen dataset. The results demonstrated that the proposed method can effectively extract road centerlines in a complex urban environment with 91.4% correctness and 80.4% completeness.

1. Introduction

With the development of digital cities and smart cities, constructing a semantically tagged 3D city model is becoming increasingly important. It is well-known that road layout is one of the primary compositions in a 3D city model and that the topological and geometric information provides a full understanding of the entire city. Additionally, this information could also be used in other aspects, such as in city planning, navigation and traffic safety. Due to the significance of road information, there has been a surge of research interest in road extraction in recent years.

Four decades of road extraction research have passed, dating back to at least Bajcsy and Tavakoli (1976). From that time, a number of achievements on road extraction methods from satellite images have been made. Significant among the techniques applied are the learning methods (Boggess, 1993; Mnih and Hinton, 2010), dynamic programming methods (Gruen and Li, 1995, 1997), active contours methods (Laptev et al., 2000; Agouris et al., 2001), heuristic bottom-up grouping methods (Poullis and You, 2010; Miao et al., 2013; Poullis, 2014), and CRF model based methods (Wegner et al., 2013; Montoya-Zegarra et al., 2015). Although these methods can realize road extraction, three problems are yet to be resolved due to the characteristics of the satellite image. These problems are as follows: (1) occlusion caused by trees; (2) "different objects with same image" or "same object with different images"; and (3) shadows caused by tall buildings (Poullis and You, 2010; Weng, 2012; Hu et al., 2014; Montoya-Zegarra et al., 2015).

In order to avoid the aforementioned problems, several studies attempted to extract road from LiDAR point clouds. Airborne LiDAR is a new technology which has been developing quickly in recent years. This method can directly obtain 3D coordinate information of objects and is easier for modeling. Moreover, airborne LiDAR

* Corresponding author.
E-mail addresses: huizhenyang2008@163.com (Z. Hui), hyj_06@163.com (Y. Hu), sgjin@shao.ac.cn (S. Jin), ziggah78@yahoo.com (Y.Z. Yevenyo).

http://dx.doi.org/10.1016/j.isprsjprs.2016.04.003
0924-2716/

can produce multiple echoes, and this feature weakens the influence of occlusion caused by trees. The LiDAR point cloud also contains the intensity information, which helps to improve the accuracy of road extraction. Owing to these advantages, researchers have developed some methods of extracting road from airborne LiDAR point clouds. For instance, Clode et al. (2004) used a hierarchical classification method to convert LiDAR data into a grid digital surface model (DSM). The road candidate points were obtained by filtering from a given distance to the digital terrain model (DTM) and intensity value. Road patches were later connected to a road network through a morphological closing operation. However, the correctness of this method is not high, especially around bridge. In order to improve the efficiency of this method, Clode et al. (2007) introduced another algorithm called phase coded disk (PCD) to vectorize the road network image. Compared to the hierarchical classification method, the PCD approach could obtain better results. Vosselman and Zhou (2009) offered a method relying on the curbstone detection. As curbstones are usually located between the road surface and adjacent pavement, the road sides could be obtained through the detection of locations with a small vertical jump caused by curbstones. The result showed that the performance of this method depends on curbstones occlusion conditions. Zhu and Mordohai (2009) converted the road extraction into a minimum cover problem. This approach does not need heavy computation and could be used for handling large-scale data. Zhao et al. (2011) applied an expectation maximization (EM) algorithm to obtain a road candidate image. These authors developed a radius-rotating method to find road intersections and sliced roads from these places. A total least squares line fitting was later used to obtain road centerlines. Although Zhao et al. (2011) obtained satisfactory completeness and correctness in linear road extraction, their application to curvilinear road extraction was still limited. Boyko and Funkhouser (2011) described a road extraction method that can address a large number of points with high correctness and completeness. However, this method needs an approximate 2D map of the road network as input. Zhao and You (2012) developed a template fitting and field voting method whereby elevated roads could also be extracted. Hu et al. (2014) proposed a method called MTH, which represented three main famous algorithms, namely, Mean shift, Tensor voting and Hough transform. The mean shift algorithm was used for clustering road center points. To enhance salient linear features, the tensor voting algorithm was applied. Finally, the Hough transform algorithm was used to extract road centerlines. Compared with the phase coded disk (PCD) (Clode et al., 2007) method and template matching (TM) (Hu and Tao, 2005), the MTH method yielded the best outcome. Recently, Li et al. (2015) offered a semi-automatic approach to extract road networks. Firstly, road seeds were manually selected, and a region-growing algorithm was used to obtain the initial road area. Next, road centerlines were extracted using the fast parallel thinning algorithm. By combining the automatic algorithm with manual modification, incorrectly extracted roads could be removed.

Although a number of advancements in road extraction from airborne LiDAR point clouds have been made, there are still two notable unsolved problems. One is how to obtain accurate road point clouds. Many studies extract road point clouds by setting an elevation difference threshold and an intensity threshold (Clode et al., 2007; Choi et al., 2008). Compared to the elevation difference threshold, the intensity threshold has a direct impact on the extraction outcome. Clode et al. (2004) determined the intensity threshold experimentally. In order to obtain a more accurate intensity threshold, Clode et al. (2007) tried sample training. Choi et al. (2008) first selected several accurate road seeds from a point cloud referenced to an aerial image and then calculated the mean and variance of these points' intensities. The maximum threshold was set to the mean plus the variance, while the minimum threshold was set to the mean minus variance. Xu et al. (2009) used a histogram to determine the intensity threshold. Although all these methods could obtain the intensity threshold, the results are not optimal and require too much human intervention. Thus, developing an efficient way to calculate the intensity threshold automatically is still challenging.

The other difficulty is how to avoid the influence of attached areas (e.g., parking lots and bare grounds) on road extraction. Due to the similarity of elevation and intensity between the road and attached areas, it is difficult to detach them. Zhao et al. (2011) tried to eliminate wrongly extracted road centerlines formed by parking lots using voting based on road directions. This method obtained high correctness and completeness for linear roads, but its ability for curved road extraction is limited. Later, Zhao and You (2012) proposed another novel method by first designing several road templates with different directions and widths. Next, template fitting was carried out to each point. Finally, the fielded voting was performed to determine road width and direction to avoid the interference of attached areas. Hu et al. (2014) adopted the tensor voting algorithm to enhance road linear saliency. By setting the saliency threshold, non-road areas were eliminated. This method is theoretically sound but requires a large amount of calculation.

In order to improve the accuracy and efficiency of road extraction from airborne LiDAR point clouds, this paper proposes a novel road extraction method. This method is abbreviated as SRH, which indicates the use of three key algorithms: skewness balancing, rotating neighborhood, and hierarchical fusion and optimization. SRH is a multi-level method which can be applied not only to straight road extraction but also to curved road extraction. In this paper, these three main algorithms are given in Section 2. Section 3 presents several tests using the Vaihingen dataset provided by the ISPRS and another three datasets used in practice, and the study's conclusions follow in Section 4.

2. Method and algorithm

Fig. 1 depicts the flowchart of the proposed method, which includes four steps, namely ground point filtering, road point extraction, narrow road removal and road network extraction. The novel contributions of this paper mainly concentrate on the latter three steps. Essentially, the SRH is a multi-level method which is processed in a bottom-up fashion. Montoya-Zegarra et al. (2015) notes that heuristic bottom-up methods (e.g., Poullis and You, 2010; Miao et al., 2013) would make errors propagate throughout the stages of the model. However, in this paper, the outcome of each hierarchy improves and errors do not accumulate.

The multi-resolution hierarchical classification algorithm proposed by Chen et al. (2013) was first applied to ground point filtering. This filtering algorithm has been proved to be more accurate and robust in complicated environments.

In order to extract road points, three constraints, namely, the intensity constraint, the point density constraint and the connected area constraint mentioned by Xu et al. (2009), were adopted to classify road points from a ground point cloud. As the intensity constraint is the dominant factor affecting the road point extraction result, this study primarily focuses on the intensity constraint. In fact, the skewness balancing algorithm used for filtering was adopted as a new way to calculate the intensity threshold. Although the skewness balancing has been widely used for segmenting the ground points from object points (referred to as filtering), such as the method proposed by Bartels and Wei (2006) and the method proposed by Crosilla et al. (2013), skewness

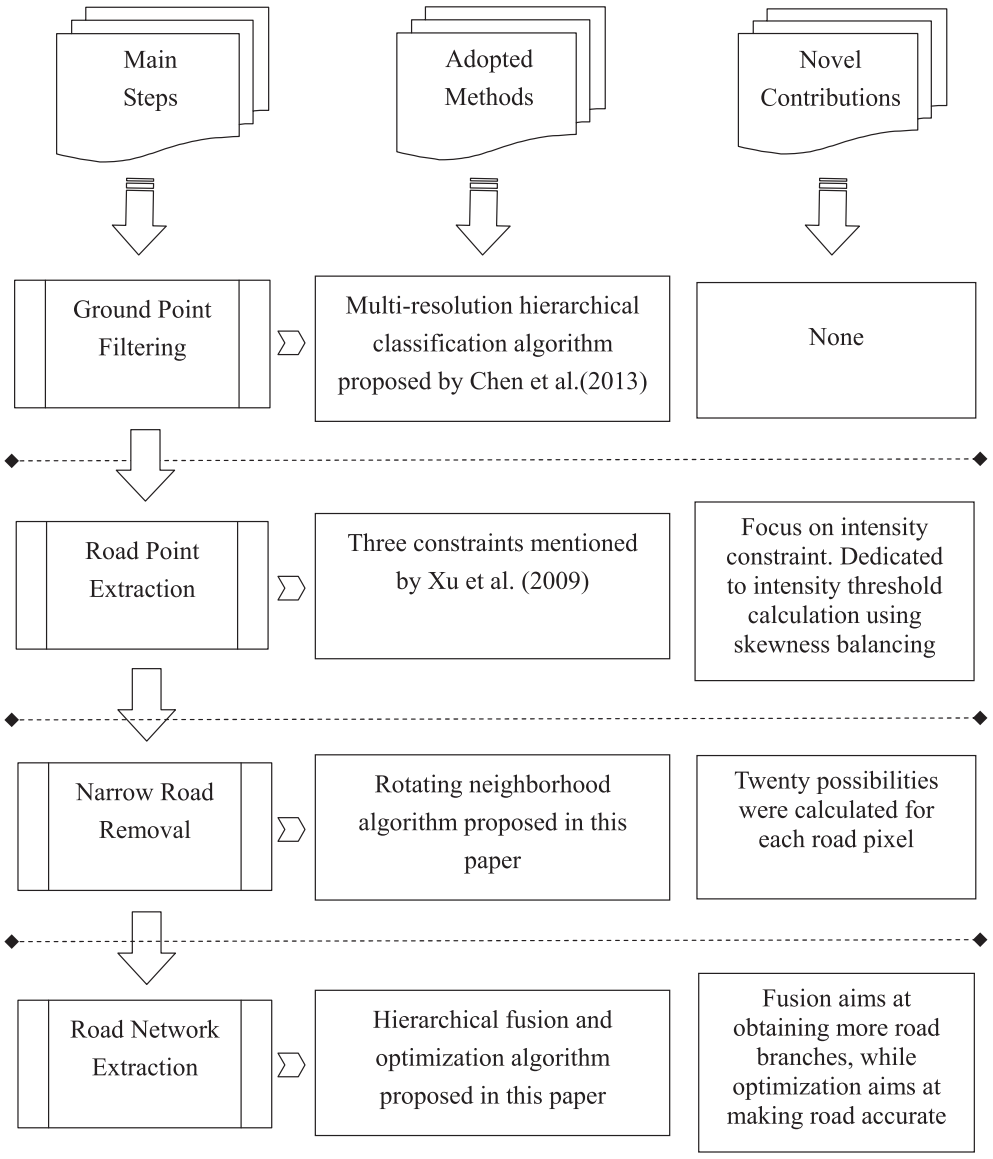

Fig. 1. Flowchart of the proposed method.

balancing is for the first time being adopted to reject non-road points from ground points.

Another novel contribution is the rotating neighborhood algorithm developed in this paper, which is used to remove narrow roads, such as corridors or sidewalks. The rotating neighborhood algorithm is very different from some existed publications using a road template (Zhao et al., 2002; Kim et al., 2004; Lin et al., 2011). In this study, five templates with different centers are fixed around the selected road pixel, and the surrounding neighbors are rotated every time. Hence, this algorithm is much easier to realize with less computation than applying the road template at different orientations every time. Meanwhile, five different templates with four different orientations mean that every pixel will be calculated for twenty possibilities to test whether it is road. Therefore, the rotating neighborhood algorithm will be more robust to some changing roads thereby making the extraction result more accurate.

The final step was based on road network extraction. This paper developed a hierarchical fusion and optimization algorithm. Although the hierarchical approach has been widely used, such as Kurtz et al. (2012) and Kurtz et al. (2014), the proposed algorithm is totally different from the previous uses. These publications focus only on how to fuse more information together which would make errors accumulate. In addition to the fusion aspect, this study spends more effort on the optimization aspect. While more road branches are fused together, making the fused results more accurate is the focus of this research. In view of this, road junction finding regulation and road centerline optimization rules are developed to get rid of the influence of attached areas (e.g., parking lots, grass lands, and bare grounds).

As mentioned previously, the following will introduce three novel contributions of this paper, namely, determining optimal intensity threshold by applying the skewness balancing algorithm, removing narrow roads by adopting the rotating neighborhood algorithm and extracting road networks using the hierarchical fusion and optimization algorithm.

2.1. Determining optimal intensity threshold

Among the intensity, point density and connected area constraints, the intensity constraint is the dominant factor affecting the road extraction result. This property is observed because the

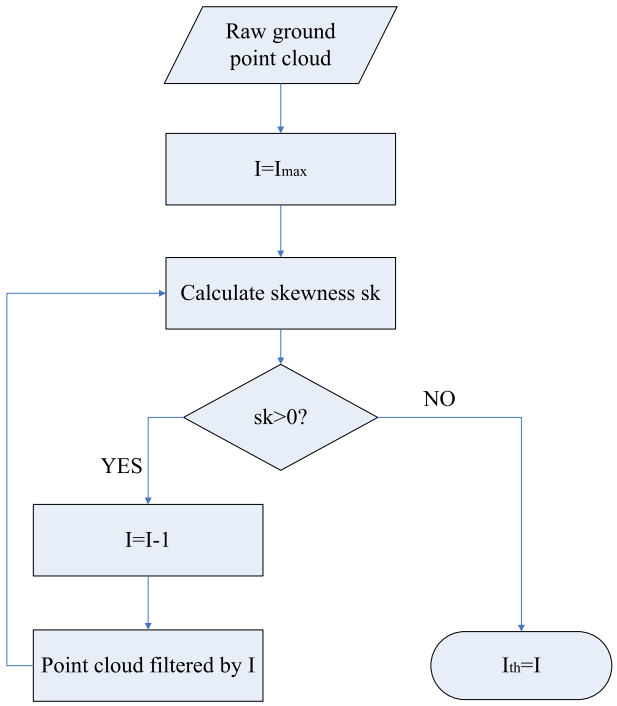

Fig. 2. Flowchart of intensity threshold determination.

material of the road is consistent and obviously different than that of bare earth, leading to a distinct difference of return intensity between the road and the surrounding ground. Considering this difference, the road points can be classified from ground points by setting an intensity threshold. However, conventional intensity threshold setting methods always depend on experience, which usually results in an approximated range. Hence, it is difficult to set an optimal intensity threshold, making it impossible to obtain "pure" road points. To address this problem, this paper tries to obtain an optimal intensity threshold automatically based on the skewness balancing, which has been used only for filtering in some existed publications.

The skewness balancing was originally formulated by Bartels et al. (2006) to separate ground and non-ground points. This algorithm is based on two assumptions: one is that the elevation of ground points is normally distributed, meaning that skewness (*sk*) is equal to zero (Duda et al., 2011); the other is that the distribution of the raw point cloud is positively skewed due to the disturbance of object points, which means *sk* is greater than zero. After removing these object points, the normally distributed ground point cloud can be achieved (Bartels and Wei, 2006). This paper adopts similar ideas and makes the following assumptions:

① "Pure" road points' return intensity values are normally distributed, i.e., $sk = 0$.
② Non-road points' return intensity values lead raw ground points' intensity values into positive skewness distribution, i.e., $sk > 0$.

The specific algorithm is described as follows:

First of all, intensity threshold I is set to the maximum value of the raw ground points' intensity, and *sk* of the raw ground point is calculated. If $sk > 0$, the intensity threshold is tuned as $I - 1$, and the raw ground point is filtered by this new threshold. This process iterates until the skewness of the point cloud is no longer greater than zero. The final I is the optimal intensity threshold for classifying road points from ground points. The flowchart of this algorithm is depicted in Fig. 2.

As shown in Fig. 3(a), the skewness of the initial ground point intensity for the dataset of Vaihingen is 0.6915, and its probability density function (PDF) belongs to a positive distribution, satisfying the requirement of the previous assumption that raw ground points' intensities have a positive skewness distribution. When the skewness balancing algorithm was employed, the PDF of the point cloud tended to be a normal PDF with skewness of −0.0091 as shown in Fig. 3(b). Meanwhile, the optimal intensity threshold was obtained as 71.

2.2. Removing narrow roads

The road point cloud was obtained by adopting the intensity, point density and connected area constraints (Xu et al., 2009). To apply some image processing techniques, the road point cloud was first rastered as shown in Fig. 4. It was found that although most roads were extracted, the road network contained too many narrow roads, which are corridors leading to parking lots or sidewalks between residential quarters. These roads are not the main roads that are meant to be extracted. For this reason, the rotating neighborhood algorithm was proposed to remove these narrow roads.

The basic idea of the rotating neighborhood algorithm is to set five minimum road templates. By calculating the ratio of road pixels within the template to the road template itself, the selected

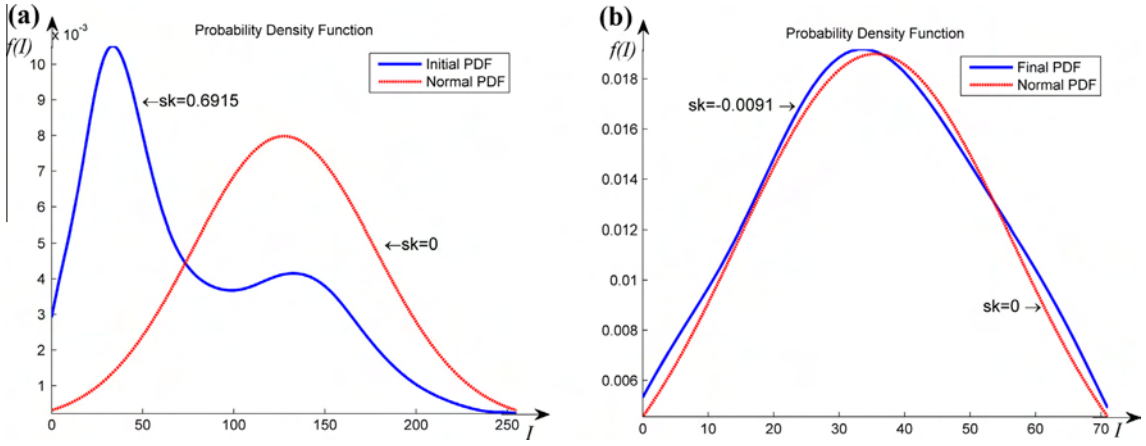

Fig. 3. PDF of intensity of point cloud: (a) PDF of intensity of raw ground points and corresponding normal PDF; and (b) PDF of intensity of filtered points and corresponding normal PDF.

Fig. 4. Initial road rastered image. The road point cloud was first projected onto the XY plane and rastered into a binary image. Then a morphological closing operation was carried out to fill some holes. Finally, four connected analysis was applied to eliminate some non-road areas.

road pixels with maximum ratio less than the threshold will be marked as narrow road and removed. As shown in Fig. 5, the length L and width W of the five road templates and the side length B of the road square neighborhood should meet the criteria expressed in Eq. (1):

$$\begin{cases} L = 2 * W - 1 \\ B = 2 * ceil(\sqrt{L^2 + W^2}) + 1 \end{cases} \quad (1)$$

where $ceil(x)$ is used to return the smallest integral value that is not less than x. It is obvious to find that once the width W is set, the road template can be determined. In this paper, W was set to 5 m, and then L was calculated as 9 m. Hence, the minimum road template was determined as 5 m × 9 m, and the side length B of the road square neighborhood was calculated as 23 m.

The five road templates are fixed around the selected road pixel, while the road square neighbors rotate at four different orientations. Thus, twenty different ratios can be calculated for each road pixel. The maximum ratio T (Eq. (2)) is selected to be the largest one among them.

$$T = \max\left(\frac{S^i_{alpha}}{L * W}\right) \quad alpha = 0^\circ,\ 30^\circ,\ 60^\circ,\ 90^\circ; \quad i = 1,2,3,4,5 \quad (2)$$

where S^i_{alpha} is the area of road pixels within the template whose center is i, while the orientation of the square neighbor is *alpha*.

It must be noted that for each road pixel twenty possibilities were calculated to test whether it is narrow road or not. If the maximum ratio T is less than the threshold, the road pixel is rejected as narrow road. In this paper, the ratio threshold is set to 0.78, which is a user-defined constant.

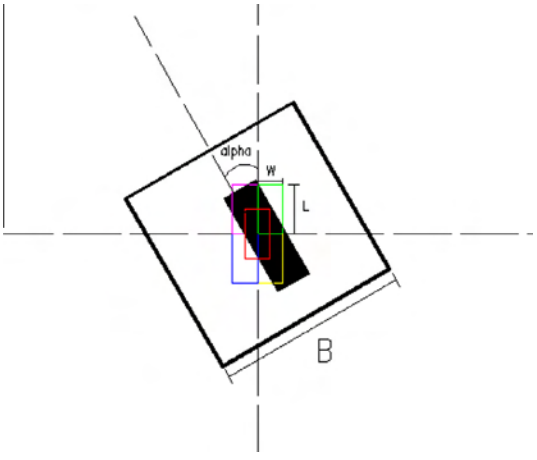

Fig. 5. Five road templates of different centers with square neighbor at *alpha* orientation. The black area represents road pixels, white area surrounded by a black box represents its square neighbor, and five rectangular boxes with different colors represent road templates of different centers.

2.3. Hierarchical fusion and optimization

After removing narrow roads, the binary road image still contains some attached areas, such as parking lots, low grass lands, or bare grounds, which have similar intensities and elevations as the road. These similar features make it difficult to remove these attached areas from road areas. However, there is one distinct difference between attached areas and road areas in that roads are always elongated while the attached areas are generally irregular in shape. Based on this characteristic these attached areas can be detached.

2.3.1. Hierarchical road extraction

The morphological opening operation can retain areas suitable for structural element (SE) and remove areas smaller than SE. As roads are always in a long ribbon distribution, they can be extracted well using linear SE. Nonetheless, when the road is varying in direction, only those roads with the same direction in linear SE's direction can be extracted. In order to extract roads in all directions, linear SE with multiple directions was set to do a morphological opening operation with binary road image (Tao et al., 2010). The multi-direction linear SE can be defined according to Eqs. (3)–(5), with Fig. 6 vividly depicting its shape.

$$SE_{L,\alpha_i} = \begin{cases} y_i = x_i \tan(\alpha_i) & x_i = 0, \pm 1, \cdots \pm (L-1)\cos(\alpha_i)/2 \quad if\ |\alpha_i| \leqslant 45^\circ \\ x_i = y_i \cot(\alpha_i) & y_i = 0, \pm 1, \cdots \pm (L-1)\sin(\alpha_i)/2 \quad if\ 45^\circ < |\alpha_i| \leqslant 90^\circ \end{cases} \quad (3)$$

$$f = \bigcup_{i=-9}^{9} IM \circ SE_{L,\alpha_i} \quad (4)$$

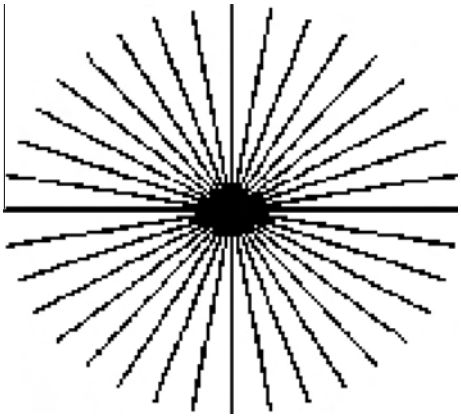

Fig. 6. Multi-direction linear SE sketch map.

$$\alpha_i = 10^\circ \times i \quad (5)$$

where SE_{L,α_i} is the multi-direction SE, L is the length of SE, α_i is direction angle, IM is the binary road image, and $\circ$ represents morphological opening operation.

In addition to the direction of linear SE influencing the result of road extraction, the length of the linear SE is also significant. Fig. 7 shows the difference between two road extraction results using two linear SEs of different lengths.

Fig. 7(a) above shows that the longer linear SE performs better on long linear road extraction. Moreover, the extraction result was barely affected by attached areas, such as parking lots, grass lands and bare grounds. Conversely, the extraction outcome had poor road integrity and lacked road details. This outcome is observed because short roads were filtered out by the long linear SE. Further, the long linear SE had little ability to extract short curvy roads. In contrast, the shorter linear SE was able to extract more roads and to keep the integrity of the road. However, the road extraction result was more affected by attached areas, such as the areas marked by red circles in Fig. 7(b).

To make full use of the strengths of both the long and the short linear SE, this paper adopts a hierarchical road extraction method. In other words, several SEs of different lengths were used to yield different road extraction outcomes of different levels.

2.3.2. Road centerlines fusion and optimization

Road centerlines can reflect the basic road location information and connected topological relationship. This paper adopts an optimized skeletonized algorithm to extract road centerlines from road images generated in Section 2.3.1. The algorithm proposed by Telea et al. (2004) can maintain road topological relationships well and does not introduce redundant road branches. In order to make the final road centerlines possess anti-interference and high integrity, road centerlines of different levels need to be fused and optimized. As shown in Fig. 8, roads extracted by the longest SE are defined as level 1. With the decreasing length of an SE, the hierarchy number increases. The hierarchical fusion and optimization are performed in a bottom-up fashion, where the outcome of each level is fused and optimized with that of the previous level. This process iterates until the preset shortest linear SE is adopted. In each iteration, four main steps need to be carried out as follows:

(1) Classify road points

In this paper, a road junction refers to the point crossed by two or more road centerlines. In contrast, there are two other types of road points, namely road endpoints and road connection points. As the road junctions are crucial in realizing the short road branch removal and attached area distinguishing, they need to be marked first from the road centerline image.

As shown in Fig. 9, R_0 represents the road point that needs to be classified. Four connected analysis to R_0's 24 neighbors is performed and the number of connected components is calculated as n. The relationship between n and the type of road pixel (R_0) is defined as follows:

(i) If n is equal to 1, the R_0 pixel represents a road endpoint;
(ii) If n is equal to 2, the R_0 pixel represents a road connection point;
(iii) If n is greater than 2, the R_0 pixel represents a road junction.

(2) Remove short road branches

In order to extract the main road network, several short road branches need to be removed first. To calculate the length of road branches, each of them should be tracked. The tracking begins from the road endpoint and ends at another road endpoint or at a road junction. By setting a road length threshold some short road branches are removed. Meanwhile the corresponding marks of road junctions are also removed.

(3) Distinguish attached area

Parking lots, low grasslands and bare grounds are regarded as attached areas. As mentioned at the beginning of Section 2.3, these attached areas seriously affect the road extraction result; thus, these areas should be detached from road areas. Due to the non-ribbon-like shape of these attached areas, the skeletonized road

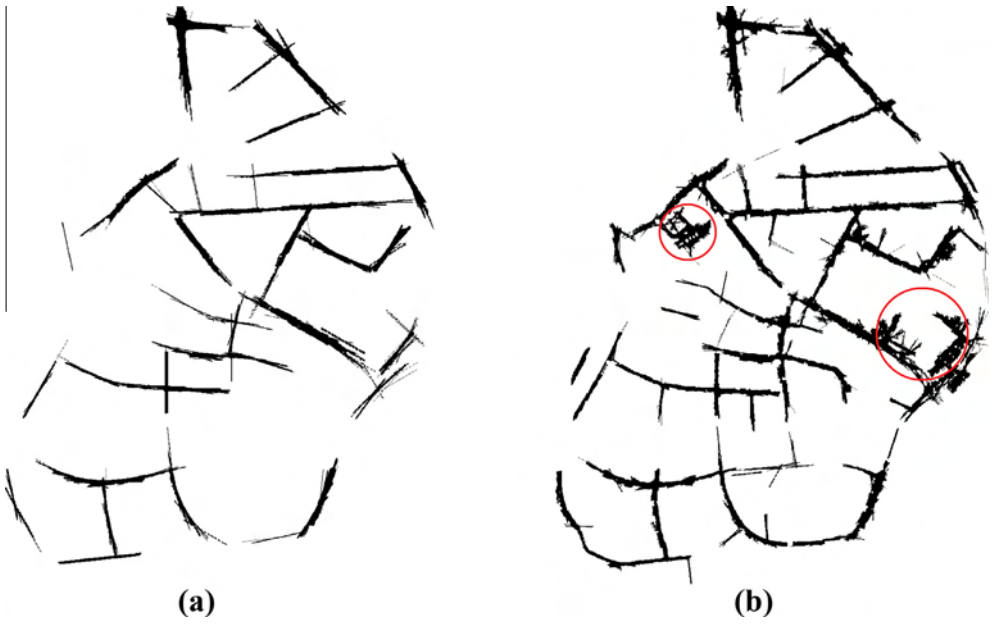

Fig. 7. Road extraction results using two linear SEs of different lengths: (a) the length of linear SE is 91 m; and (b) the length of linear SE is 51 m. The red-circle labeled areas in (b) indicate attached areas. The two linear SEs are both used to do a morphological opening operation with the binary road image, which consists of an erosion operation followed by a dilation operation. (For interpretation of the references to colour in this figure legend, the reader is referred to the web version of this article.)

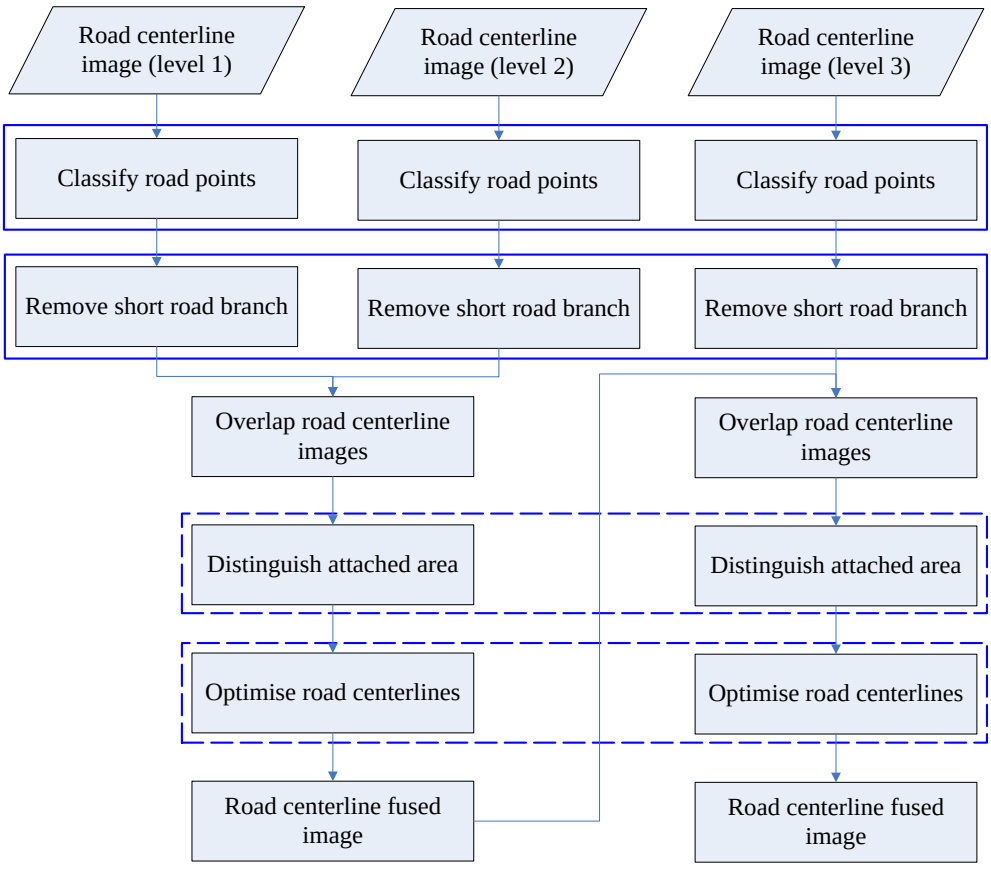

Fig. 8. Flowchart of hierarchical fusion and optimization algorithm.

centerlines will cross each other to form many road junctions as shown in Fig. 10(c). Consequently, attached areas can be distinguished according to the number of road junctions in the local area.

The attached area discrimination rule is defined as follows: the three nearest road junctions from each hierarchy and its successive hierarchy are found and the maximum chessboard distance among them is calculated. If the maximum chessboard distance is less than the threshold, the corresponding road area is marked as attached area. The chessboard distance is defined in Eq. (6) as:

$$d[(i,j),(h,k)] = \max(|i-h|,|j-k|) \tag{6}$$

where (i,j) and (h,k) are the pixel positions of two different road junctions, respectively.

(4) Optimize road centerlines

Road centerline optimization includes two aspects, namely, the attached area optimization and the non-attached area optimization. The non-attached area refers to road area without influence of, for example, parking lots, bare ground, and grass land. The optimization process was conducted on the fused road centerlines image.

(i) Attached area optimization

In the attached area, the optimization principle is removing road centerlines of the upper level (hierarchy using shorter linear SE) and preserving road centerlines of the lower level (hierarchy using longer linear SE). To this end, the road junctions in the attached area and road branches connected to them in the upper level are removed while maintaining corresponding road branches of the lower level. Thus, it is implicitly assumed that road centerlines of the lower level are more accurate than the ones of the upper level in the attached area.

(ii) Non-attached area optimization

The road centerline of the same road at different levels in a non-attached area is also likely to be slightly offset. Thus, on the fused image some road centerlines may diverge or be adjacent in the stack, but generally, these offsets are only slight as shown in Fig. 11(b). Hence, a morphological closing operation is first adopted to fill these small holes caused by offsets, and the optimized skeletonized algorithm is subsequently applied to the result once again. In this way, the road centerlines of non-attached areas are optimized.

3. Experiment and analysis

The proposed method was applied to the Vaihingen dataset provided by the International Society for Photogrammetry and Remote Sensing. The Vaihingen dataset was captured with the Leica ALS50 system, and its average point density is 4 points/m^2 (Cramer, 2010). Roads in this city are varying in widths with cars on the road, and there are also some high trees shielding the road. Moreover, some attached areas, such as parking lots, grass lands, and bare grounds are along the road. Therefore, this dataset has a very good representation of features for testing road extraction methods.

3.1. Binary road image

With the help of the skewness balancing algorithm, the road intensity threshold for the Vaihingen dataset was calculated as 71. In this paper, the minimum road template was set as

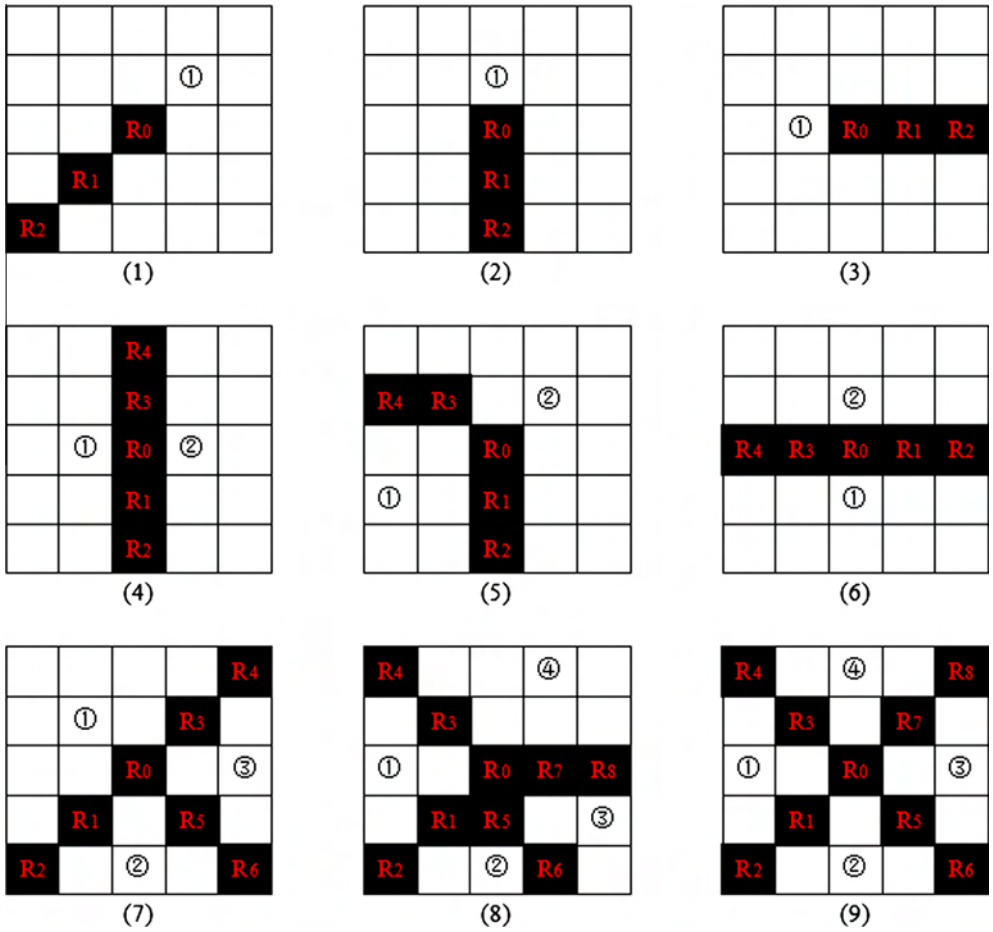

Fig. 9. The relationship between the type of road pixel and the number of connected components. Road endpoint: (1), (2) and (3). Road connection point: (4), (5) and (6). Road junction: (7), (8) and (9). R_i represents road pixel. R_0 is the road pixel to be classified. Four connected analysis results of (1)–(9) are 1, 1, 1, 2, 2, 2, 3, 4 and 4, respectively.

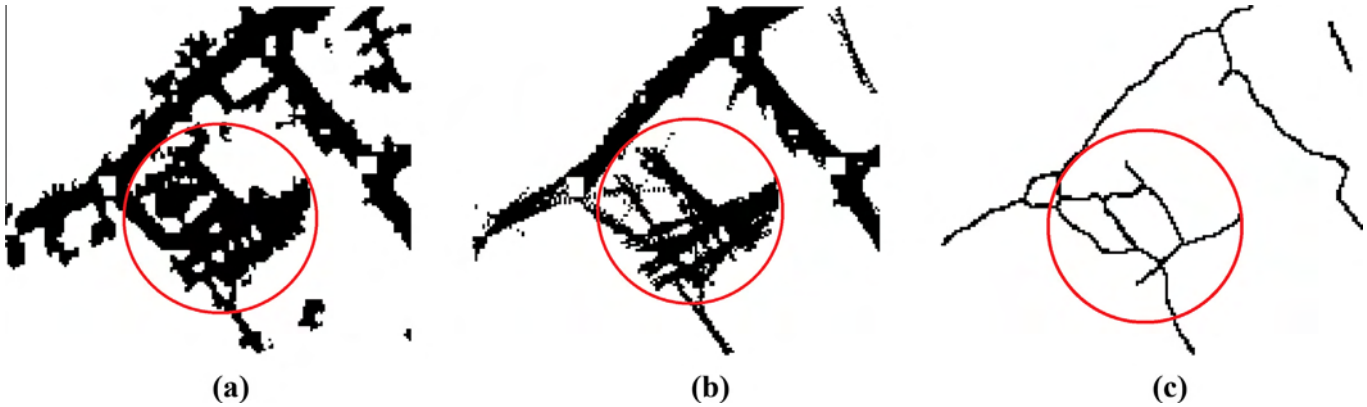

Fig. 10. Process of road centerline extraction: (a) initial road binary image; (b) extracted roads using linear SE; and (c) extracted road centerlines using the optimized skeletonized algorithm. The red circle labeled area in (c) is the attached area. Many road junctions can be found in this area. (For interpretation of the references to colour in this figure legend, the reader is referred to the web version of this article.)

5 m × 9 m, which means that any road smaller than the road template will be removed. The final binary road image for Vaihingen is shown in Fig. 12.

3.2. Hierarchical fusion and optimization

The core content of this paper is the hierarchical road centerline fusion and optimization. Before doing this action, road centerlines of different hierarchy are extracted first. Here, four linear SEs of different length, namely 91 m, 71 m, 51 m and 31 m were utilized to extract roads. The four road centerline extraction outcomes of different hierarchies are shown in Fig. 13.

From Fig. 13, it can be observed that the shorter linear SE extracted more road centerlines. However, there is a greater likelihood that attached areas could be misclassified as roads. To solve this problem, road centerlines are fused and optimized in a bottom-up fashion. The outcome of each iteration is shown in Fig. 14.

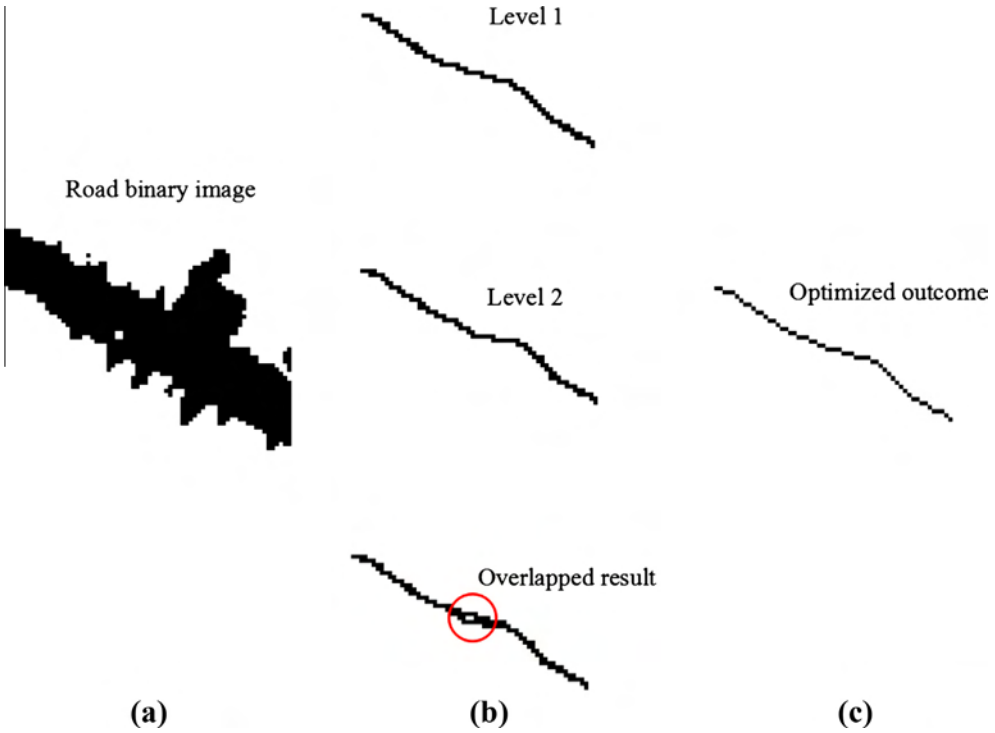

Fig. 11. Process of road centerline optimization in non-attached area: (a) road binary image; (b) road centerlines of different level skeletonized from (a); and (c) optimized road centerline. The red circle labeled in (b) indicates the hole caused by offset of road centerlines of different level. (For interpretation of the references to colour in this figure legend, the reader is referred to the web version of this article.)

Fig. 12. Road binary image after removing narrow roads.

During the fusion and optimization process as shown in Fig. 14, more roads were fused together, while roads caused by attached areas were filtered. This is because by calculating chessboard distance between the road junctions, attached areas can be effectively discriminated, thereby filtering spurious roads caused by these areas. Another characteristic is that the extraction outcome is very "clean" and has a good integrity. In other words, the result does not contain many small fragmented roads. This is because the present study applies the rotating neighborhood algorithm to the initial road binary image to first remove roads smaller than the minimum road template.

3.3. Time required and parameter study

Three main steps, namely intensity threshold calculation by applying the skewness balancing algorithm, narrow roads removal by adopting the rotating neighborhood algorithm and road centerline extraction using the hierarchy fusion and optimization algorithm, are involved in this novel road centerline extraction method. Table 1 shows the time required for each step. Here, the test was performed on Intel Core™ i5 CPU with 2 GB of main memory. The intensity threshold calculation covered 3,445,546 ground points taking 1.1 min. In the second step of narrow road removal, twenty possibilities were calculated for every road pixel to test whether it was narrow road or not. However, owning to the efficient principle of the rotating neighborhood algorithm, this step took only a few minutes. Similarly, although the last step needs to fuse and optimize four hierarchies' results, it does not take much time.

Six parameters, as shown in Table 2, need to be preset for this study. Although the extraction outcome may be different if any one of these parameters is changed, this paper focuses only on two parameters, namely L_{max} and L_{min}, which indicate the longest linear SE and the shortest linear SE because these two parameters are the dominant factors affecting the result. In this paper four linear SEs of different lengths were set in arithmetic progression, namely 91 m, 71 m, 51 m, and 31 m. In comparison, this study tested the dataset using another three groups of linear SEs with different L_{max} and L_{min}. Those results are shown in Fig. 15. By visual inspection of Fig. 15, it can be observed that different combinations of linear SEs lead to different extraction results. Further, longer L_{max} values obtain more straight roads, but extract less road

Fig. 13. Road centerline extraction outcomes of different hierarchy. The lengths of linear SE for (a)–(d) are 91 m, 71 m, 51 m and 31 m, respectively.

details. In view of this, L_{max} and L_{min} should be tuned by trial and error in order to obtain the best performance.

3.4. Result evaluation

Three indicators, namely correctness (C_r), completeness (C_p) and quality (Q), are used to quantitatively assess the extraction effect of road centerlines. These three indicators are mathematically defined in Eqs. (7)–(9) (Wiedemman et al., 1998):

$$C_r = \frac{T_p}{T_p + F_p} \times 100\% \tag{7}$$

$$C_p = \frac{T_p}{T_p + F_n} \times 100\% \tag{8}$$

$$Q = \frac{T_p}{T_p + F_p + F_n} \times 100\% \tag{9}$$

where T_p is the total length of correctly extracted roads, F_p is the total length of wrongly extracted roads and F_n is the total length of missed roads.

The evaluation references "true" road centerlines, which can be manually digitized. The experiment results show that correctness, completeness and quality are 91.4%, 80.4%, and 74.8%, respectively. In addition, the extraction results of SRH are compared to that of the MTH method proposed by Hu et al. (2014) and two other algorithms, the Phase Code Disk approach (PCD) proposed by Clode et al. (2007) and Template Matching (TM) proposed by Hu and Tao (2005), as shown in Fig. 16. Because the same data (Vaihingen dataset) was used for SRH, MTH, PCD and TM, their extraction results can be compared directly.

It can be observed from Fig. 16 that the proposed method yields the best result. This finding can be explained by the following two aspects. First, as a prerequisite for extracting accurate road center-

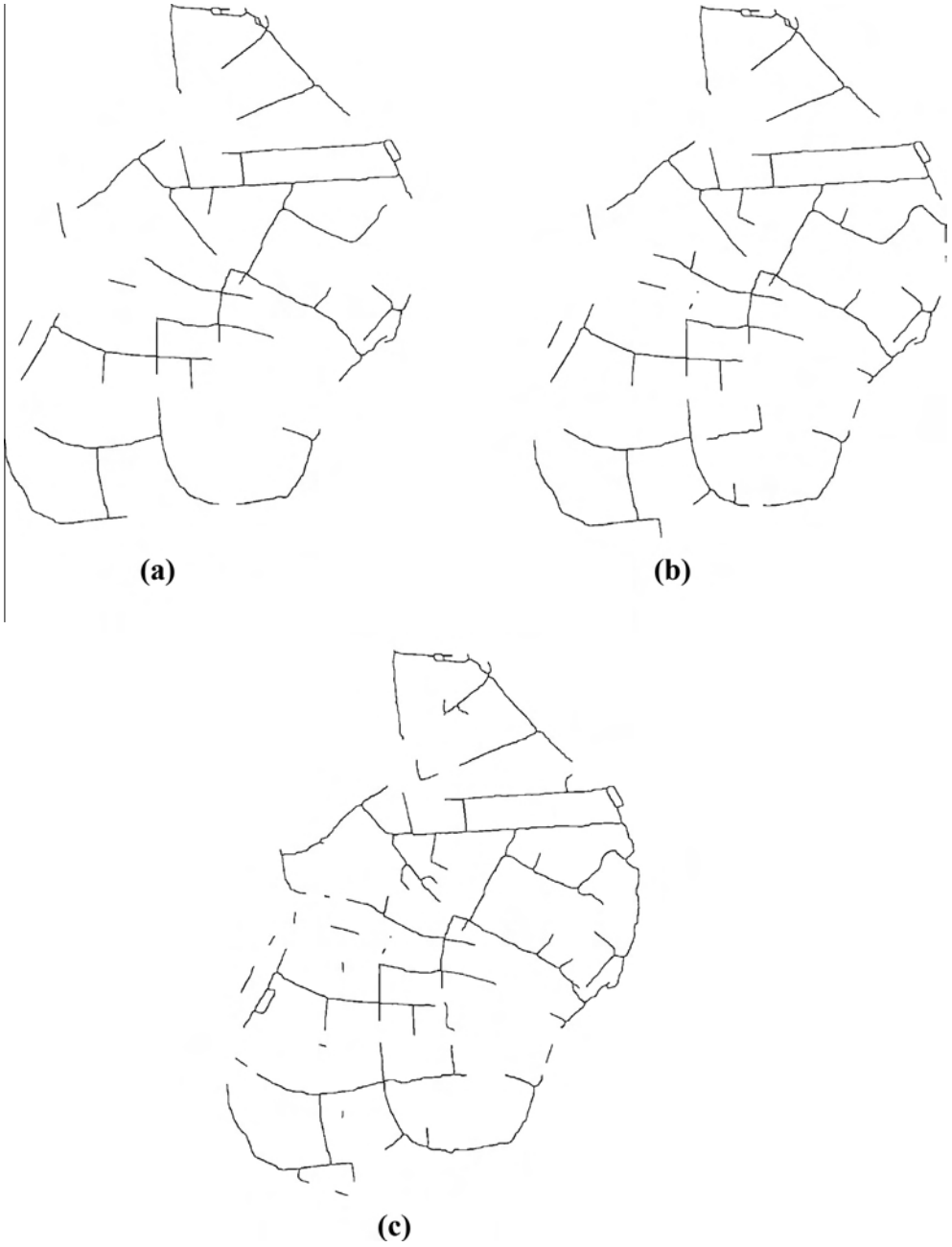

Fig. 14. The outcome of fusion and optimization at each iteration: (a) the outcome of the first iteration (level 1 with level 2); (b) the outcome of the second iteration (outcome of the first iteration with level 3); and (c) the outcome of the third iteration (outcome of the second iteration with level 4).

Table 1
The time required for each step.

Steps	Intensity threshold calculation (min)	Narrow road removal (min)	Road centerline extraction (min)
Time	1.1	5.4	10.1

Table 2
Parameters preset in this paper.

Parameters	Narrow road removal		Road centerline extraction			
	Width (m)	Area ratio	Short road branch (m)	Chessboard distance (m)	L_{max} (m)	L_{min} (m)
Values	5	0.78	40	40	91	31

lines, the skewness balancing algorithm was utilized to calculate optimal intensity threshold, thereby obtaining a "pure" and accurate road point cloud. Second, the hierarchical fusion and optimization algorithm proposed in this paper extracts a more accurate road network. Roads extracted by the longer SE are barely affected by attached areas and could be more accurate, while roads extracted by the shorter SE could contain more road details. Combining these advantages yields results with high correctness and completeness.

To further investigate the performance of the proposed method, the present study applied the SHR to another three datasets used in practice. As shown in Figs. 17(a), 18(a) and 19(a), these three datasets are located in different areas with different geographical features. The final road network extraction accuracies of these three datasets are indicated in Table 3. As shown in Fig. 17(a),

Fig. 15. Road centerline extraction results with different groups of linear SE: (a) the lengths of four linear SEs are 121 m, 101 m, 81 m and 61 m; (b) the lengths of four linear SEs are 111 m, 91 m, 71 m and 51 m; (c) the lengths of four linear SEs are 101 m, 81 m, 61 m and 41 m; and (d) the lengths of four linear SEs are 91 m, 71 m, 51 m and 31 m.

roads in test site 1 are regularly distributed. However, some parts of roads in this area are shielded by trees making these road areas have no LiDAR data (red dotted rectangle labeled areas in Fig. 17 (b)). Because of this the final extracted road network possessed some undetected roads (F_n), which led to a little lower completeness of this test site. In test site 2, there are many narrow roads between residential districts. Owing to the rotating neighborhood algorithm proposed in this paper, these narrow roads had little influence on the final road extraction result. The main problem is that the final extracted road network contained many wrongly extracted roads (F_p) making the correctness of this area to be less than desired. This is because there are many road-like areas which have similar elevation and reflection intensity to roads. Moreover, certain of these areas are also in ribbon distribution, which would hinder the proposed method in discriminating them from roads. As indicated in Table 3, both correctness and completeness of test site 3 are very poor. From Fig. 19(a) it can be found that roads in test site 3 are irregularly distributed and covered by many dense trees. By applying the skewness balancing algorithm to the point cloud of this area, the intensity threshold was calculated as 10. However, road areas were not extracted well using this threshold. As shown in Fig. 19(b), many non-road areas still exist among road areas. That is why the final road network (Fig. 19(c)) contains many wrongly extracted roads (F_p). On the other hand, due to lack of LiDAR data in many parts of the roads, many roads in this area were undetected. A higher F_n led to poor completeness.

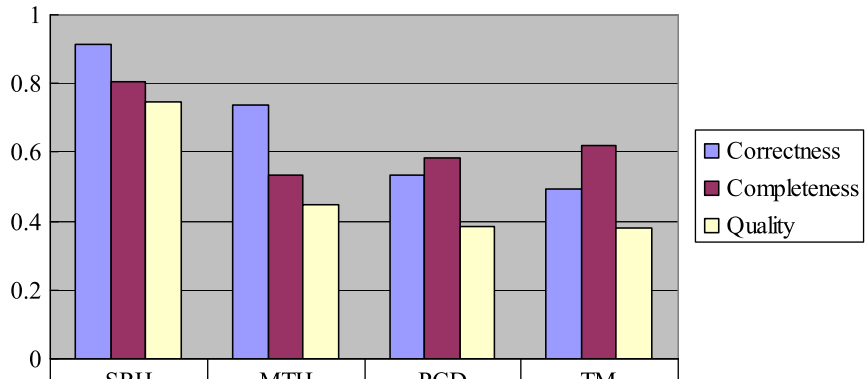

	SRH	MTH	PCD	TM
Correctness	0.914	0.738	0.532	0.495
Completeness	0.804	0.534	0.583	0.621
Quality	0.748	0.449	0.385	0.379

Fig. 16. The accuracy comparison of road centerline extraction results of the four different methods. Three indicators (correctness, completeness, and quality) of the other three algorithms (MTH, PCD and TM) are provided by Hu et al. (2014).

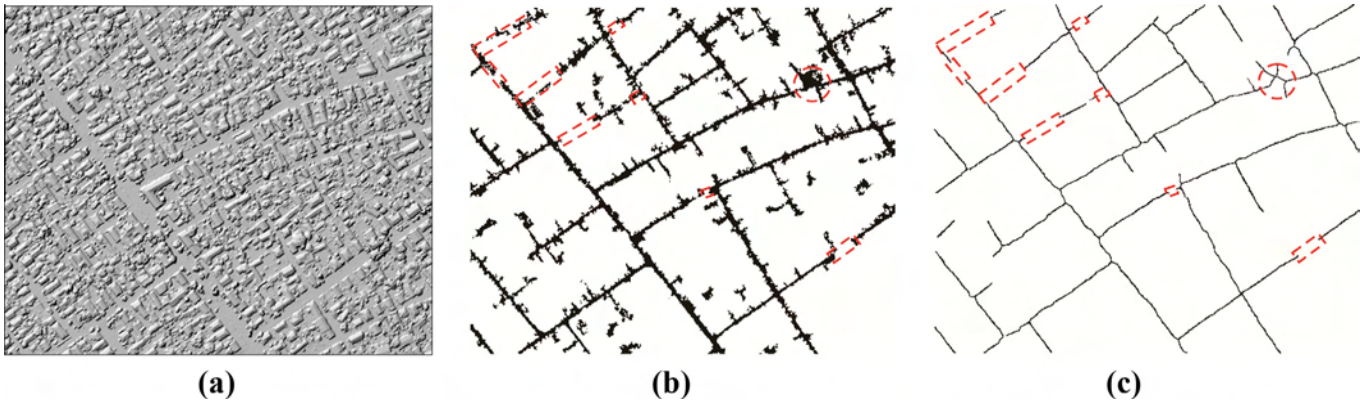

Fig. 17. (a) The shaded DSM of test site 1; (b) the binary image of road extraction result; (c) the final extracted road network. The shaded DSM in (a) was derived in Surfer 12.0 software using three-dimensional coordinates information. The areas labeled with red dotted rectangles represent the undetected road centerlines, while the areas labeled with red dotted circles labeled area represent the wrongly extracted road centerlines. (For interpretation of the references to colour in this figure legend, the reader is referred to the web version of this article.)

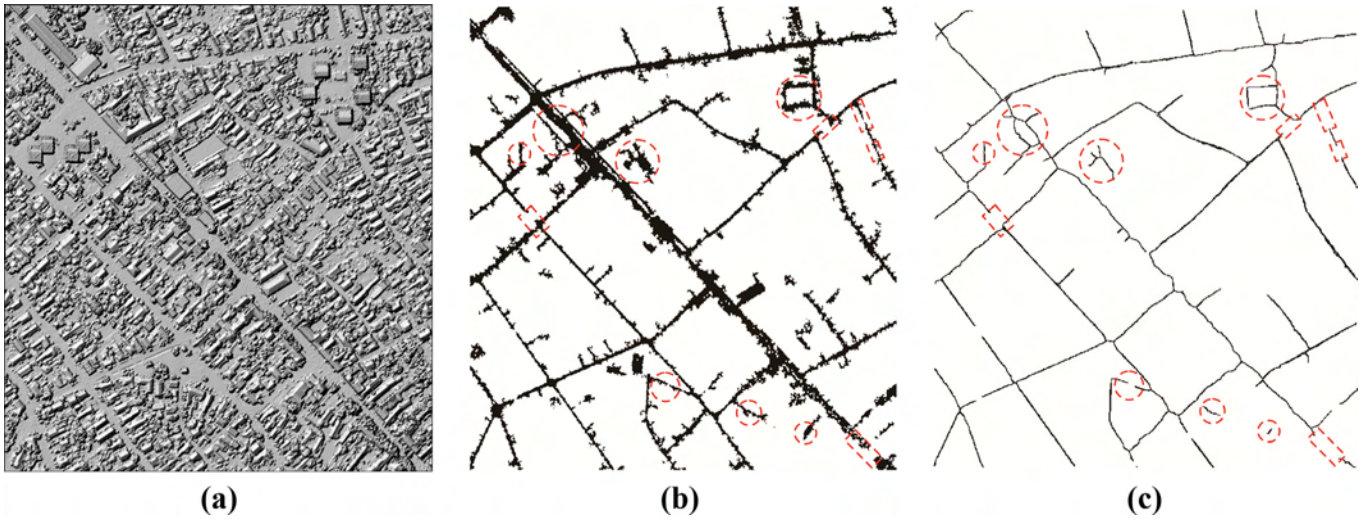

Fig. 18. (a) The shaded DSM of test site 2; (b) the binary image of road extraction result; (c) the final extracted road network. The shaded DSM in (a) was derived in Surfer 12.0 software using three-dimensional coordinates information. The areas labeled with red dotted rectangles represent the undetected road centerlines, while the areas labeled with red dotted circles labeled area represent the wrongly extracted road centerlines. (For interpretation of the references to colour in this figure legend, the reader is referred to the web version of this article.)

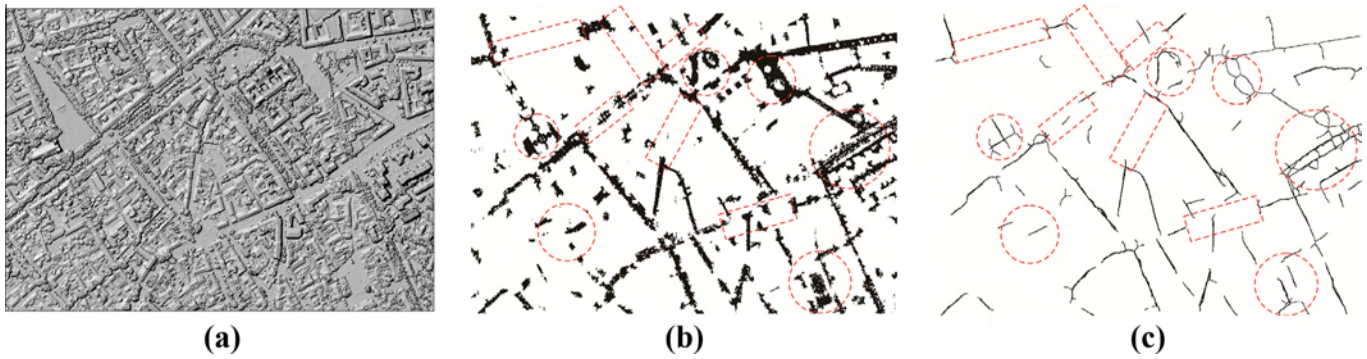

Fig. 19. (a) The shaded DSM of test site 3; (b) the binary image of road extraction result; (c) the final extracted road network. The shaded DSM in (a) was derived in Surfer 12.0 software using three-dimensional coordinates information. The areas labeled with red dotted rectangles represent the undetected road centerlines, while the areas labeled with red dotted circles labeled area represent the wrongly extracted road centerlines. (For interpretation of the references to colour in this figure legend, the reader is referred to the web version of this article.)

Table 3
Road network extraction accuracy.

	Test site 1	Test site 2	Test site 3
Correctness	0.923	0.824	0.431
Completeness	0.795	0.907	0.359
Quality	0.752	0.746	0.298

4. Conclusions

Road extraction from airborne LiDAR point clouds has been a research hotspot for several years. Many methods have been proposed in this field. However, there are still three unresolved difficulties for extracting road information from point clouds: how to extract road point cloud data purely from raw point cloud data; how to discriminate and remove narrow roads from city main roads effectively; and how to make the road extraction result free from the influence of attached areas. In this paper, a novel method (SRH) was proposed to extract road network from airborne LiDAR point cloud more effectively using three algorithms: Skewness balancing, Rotating neighborhood and Hierarchical fusion and optimization.

The skewness balancing algorithm can help obtain accurate intensity threshold, which can make the obtained road point cloud more "pure." The rotating neighborhood algorithm is proposed to help extract main roads of the city. The hierarchical fusion and optimization algorithm has two strengths: making the result robust to attached area and making the extraction of roads more possible.

SRH was tested against the Vaihingen dataset provided by the ISPRS Test Project. The results show that this method yields better performance than three other methods (MTH, TM and PCD). Another three tests using the datasets used in practice also proved the effectiveness of the proposed method. Although the proposed method could yield a promising performance, this method is susceptible to introducing wrong road branches when the road point cloud contains some "holes" caused by cars, trees, etc. Some small "holes" can be filled by the morphological closing operation; however, if the holes are too large to be filled, wrong road centerlines will be introduced. Therefore, further research is warranted to solve this problem.

Acknowledgments

The authors would like to thank the German Society for Photogrammetry, Remote Sensing and Geoinformation (DGPF) for providing the Vaihingen dataset (Cramer, 2010). http://www.ifp.unistuttgart.de/dgpf/DKEP-Allg.html.

The authors would like to thank Natural Science Foundation of China (Grant Nos: 41374017 and 11373059) and Key Laboratory of Precise Engineering and Industry Surveying, National Administration of Surveying, Mapping and Geoinformation (Project No: PF2012-21) for their financial support. The authors also express their appreciation to the anonymous reviewers for their valuable suggestions.

References

Agouris, P., Stefanidis, A., Gyftakis, S., 2001. Differential snakes for change detection in road segments. Photogramm. Eng. Remote Sens. 67, 1391–1399.
Bajcsy, R., Tavakoli, M., 1976. Computer recognition of roads from satellite pictures. IEEE Trans. Syst., Cybern. 6, 623–637.
Bartels, M., Wei, H., 2006. Segmentation of LIDAR data using measures of distribution. Int. Arch. Photogramm. Remote Sens. Spatial Inf. Sci. XXXVI (7), 426–431.
Bartels, M., Wei, H., Mason, D.C., 2006. DTM generation from LIDAR data using Skewness Balancing. In: Pattern Recognition, 2006. ICPR 2006. 18th International Conference on. 1, pp. 566–569.
Boggess, J.E., 1993. Identification of Roads in Satellite Imagery Using Artificial Neural Networks: A Contextual Approach. Mississippi State Univ. Press, Mississippi.
Boyko, A., Funkhouser, T., 2011. Extracting roads from dense point clouds in large scale urban environment. ISPRS J. Photogramm. Remote Sens. 6 (Suppl), S2–S12.
Chen, C., Li, Y., Li, W., Dai, H., 2013. A multiresolution hierarchical classification algorithm for filtering airborne LiDAR data. ISPRS J. Photogramm. Remote Sens. 82, 1–9.
Choi, Y.W., Jang, Y.W., Lee, H.J., Cho, G.S., 2008. Three-dimensional LiDAR data classifying to extract road point in urban area. IEEE Geosci. Remote Sens. Lett. 5, 725–729.
Clode, S., Kootsookos, P., Rottensteiner, F., 2004. The automatic extraction of roods from LiDAR data. Int. Arch. Photogramm. Remote Sens. Spatial Inf. Sci. 35, 231–237.
Clode, S., Rottensteiner, F., Kootsookos, P., Zelniker, E., 2007. Detection and vectorization of roads from LIDAR data. Photogram. Eng. Remote Sens. 73, 517–536.
Cramer, M., 2010. The DGPF test on digital aerial camera evaluation-Overview and test design. Photogramm.-Fernerkundung-Geoinf. 2, 73–82.
Crosilla, F., Macorig, D., Scaioni, M., Sebastianutti, I., Visintini, D., 2013. LiDAR data filtering and classification by skewness and kurtosis iterative analysis of multiple point cloud data categories. Appl. Geomatics 5, 225–240.
Duda, R.O., Hart, P.E., Stork, D.G., 2011. Patter Classification. Wiley, New York.
Gruen, A., Li, H.H., 1995. Road extraction from aerial and satellite images by dynamic programming. ISPRS J. Photogramm. Remote Sens. 50, 11–20.
Gruen, A., Li, H.H., 1997. Semi-automatic linear feature extraction by dynamic programming and LSB-Snakes. Photogramm. Eng. Remote Sens. 63, 985–995.
Hu, X., Tao, C.V., 2005. A reliable and fast ribbon road detector using profile analysis and model-based verification. Int. J. Remote Sens. 26, 887–902.
Hu, X.Y., Li, Y.J., Shan, J., Zhang, J.Q., Zhang, Y.J., 2014. Road centerline extraction in complex urban scenes from lidar data based on multiple features. IEEE Trans. Geosci. Remote Sens. 52, 7448–7456.
Kim, T., Park, S.R., Kim, M.G., Jeong, S., Kim, K.O., 2004. Tracking road centerlines from high resolution remote sensing images by least squares correlation matching. Photogramm. Eng. Remote Sens. 70, 1417–1422.
Kurtz, C., Passat, N., Gançarski, P., Puissant, A., 2012. Extraction of complex patterns from multiresolution remote sensing images: a hierarchical top-down methodology. Pattern Recogn. 45, 685–706.

Kurtz, C., Stumpf, A., Malet, J., Gançarski, P., Puissant, A., Passat, N., 2014. Hierarchical extraction of landslides from multiresolution remotely sensed optical images. ISPRS J. Photogramm. Remote Sens. 87, 122–136.

Laptev, I., Mayer, H., Lindeberg, T., Eckstein, W., Steger, C., Baumartner, A., 2000. Automatic extraction of roads from aerial images based on scale space and snakes. Mach. Vis. Appl. 12, 23–31.

Li, F., Cui, X.M., Liu, X.Y., Wei, A.X., 2015. A semi-automatic algorithm of extracting urban road networks from airborne LiDAR point clouds. Sci. Surv. Mapp. 40, 88–92.

Lin, X.G., Zhang, J.X., Liu, Z.J., Shun, J., Duan, M., 2011. Semi-automatic extraction of road networks by least squares interlaced template matching in urban areas. Int. J. Remote Sens. 32, 4943–4959.

Miao, Z., Shi, W., Zhang, H., Wang, X., 2013. Road centerline extraction from high-resolution imagery based on shape features and multi-variate adaptive regression splines. IEEE Geosci. Remote Sens. Lett. 10, 583–587.

Mnih, V., Hinton, G.E., 2010. Learning to detect roads in high-resolution aerial images. In: European Conference on Computer Vision (ECCV 2010) 11th.

Montoya-Zegarra, J.A., Wegner, J.D., Ladicky, L., Schindler, K., 2015. On the evaluation of higher-order cliques for road network extraction. In: Urban Remote Sensing Event (JURSE), 2015 Joint, pp. 1–4, March 30 2015–April 1 2015.

Poullis, C., 2014. Tensor-Cuts: a simultaneous multi-type feature extractor and classifier and its application to road extraction from satellite images. ISPRS J. Photogramm. Remote Sens. 95, 93–108.

Poullis, C., You, S., 2010. Delineation and geometric modeling of road networks. ISPRS J. Photogramm. Remote Sens. 65, 165–181.

Tao, C., Tan, Y.H., Cai, H.J., Du, B., Tian, J.W., 2010. Object-oriented method of hierarchical urban building extraction from high-resolution remote-sensing imagery. Acta Geodaetica et Cartographica Sinica 39, 39–45.

Telea, A., Sminchisescu, C., Dickinson, S., 2004. Optimal inference for hierarchical skeleton abstraction. In: Pattern Recognition, 2004. ICPR 2004. Proceedings of the 17th International Conference on, vol. 4, no., pp. 19–22.

Vosselman, G., Zhou, L., 2009. Detection of curbstones in airborne laser scanning data. Int. Arch. Photogramm. Remote Sens. Spatial Inf. Sci. 38, 111–116.

Wegner, J.D., Montoya-Zegarra, J.A., Schindler, K., 2013. A higher-order CRF model for road network extraction. In: CVPR, pp. 1698–1705.

Weng, Q.H., 2012. Remote sensing of impervious surfaces in the urban areas: requirements, methods, and trends. Remote Sens. Environ. 117, 34–49.

Wiedemman, C., Heipke, C., Mayer, H., Jamet, O., 1998. Empirical evaluation of automatically extracted road axes. In: Empirical Evaluation Methods in Computer Vision. IEEE Press, Piscataway, NJ, USA, pp. 172–187.

Xu, J.Z., Wan, Y.C., Lai, Z.L., 2009. Multi-scale method for extracting road centerlines from LIDAR datasets. Infrared Laser Eng. 38, 1009–1103.

Zhao, H., Kumagai, J., Nakagawa, M., 2002. Semi-automatic road extraction from high resolution satellite images. In: Proceedings of ISPRS Photogrammetry and Computer Vision, 9–13 September, Graz, Austria, pp. A-406.

Zhao, J.P., You, S.Y., 2012. Road network extraction from airborne LiDAR data using scene context. In: Computer Vision and Pattern Recognition Workshops (CVPRW), 2012 IEEE Computer Society Conference on., pp. 9–16.

Zhao J.P., You, S.Y., Huang, J., 2011. Rapid extraction and updating of road network from airborne LiDAR data. In: Applied Imagery Pattern Recognition Workshop (AIPR), 2011 IEEE, pp. 1–7.

Zhu, Q.H., Mordohai, P., 2009. A minimum cover approach for extracting the road network from airborne LiDAR data. In: Computer Vision Workshops (ICCV Workshops), 2009 IEEE 12th International Conference on, pp. 1582–1589.